Hypersonic Dynamic Testing of Ablating Models with Three-Degree-of-Freedom Gas Bearing

F.J. Regan* and M.V. Krumins†
Naval Surface Weapons Center, Silver Spring, Maryland

This paper presents a description of the design, construction, and operation of the Naval Surface Weapons Center three-degree-of-freedom gas bearing. The data reduction techniques used to obtain the static and dynamic moment derivatives from angular measurements are discussed and applied to wind tunnel data. These wind tunnel data were obtained from both nose-tip ablating and nonablating conical models at Mach 7.95. The results are compared with earlier tests of nonablating static models and dynamic ablating models.

Nomenclature

C_m = pitching moment coefficient, M/QSd
C_n = yawing moment coefficient, N/QSd
C_{m_α} = pitching moment derivative, $\partial C_m/\alpha$
C_{m_q} = pitch damping moment derivative, $\partial C_m/\partial(qd/2V)$
$C_{m_{p\beta}}$ = Magnus derivative, $\partial^2 C_m/[\partial\beta\partial(pd/2V)]$
C_{N_α} = normal force derivative, $\partial C_N/\partial\alpha$
C_{n_β} = yawing moment derivative, $\partial C_n/\partial\beta$
$C_{n_{p\alpha}}$ = Magnus derivative, $\partial^2 C_n/[\partial\alpha\partial(pd/2V)]$
C_{n_r} = yaw damping derivative, $\partial C_n/\partial(rd/2V)$
d = reference length, base diameter
H = angle-of-attack derivative matrix
I = transverse moment of inertia
I_x = axial moment of inertia
L = angle of side-slip derivative matrix
M = pitching moment
N = yawing moment
p = roll rate
q,r = pitch/yaw rate
$\bar{q},\bar{r},\bar{Q},\bar{R}$ = angles side-slip/attack residual vectors
Q = dynamic pressure, $\rho V^2/2$
S = reference area, $\pi d^2/4$
V = airspeed
α = angle of attack
β = angle of sideslip
δ = control angle to trim
ρ = air density

Background

IN conventional wind tunnel testing for aerodynamic loads, the model is attached to a rigid structure, often a cantilever beam. An integral part of this supporting structure is a load measurement unit. This unit measures the forces of constraint, which are assumed equivalent to the aerodynamic loads. While there is much to recommend the testing of a rigidly constrained model, such testing cannot measure the aerodynamic effects caused by rates of change of angular variables. The three-degree-of-freedom gas bearing support was designed to permit a measurement of these time-dependent loads. The gas bearing supports the model at its center of gravity, permitting unrestricted angular motion in pitch and yaw (about 7-8 deg) and unrestricted angular motion in roll.

For testing models with active and perhaps localized ablation, the three-degree-of-freedom support permits an interaction of the ablation process with the static and dynamic characteristics of the model. Such interactions are obviously impossible in the conventional static test. The major effect of ablation is to change shape and hence to superimpose a time-varying force and moment on the static characteristics of the nonablated model. Just how the ablating shape evolves depends intimately upon the model's dynamics (roll/pitch/yaw history). As the model undergoes angular motion, the windward meridian continually moves in a body frame. Postulating that this windward meridian is also the meridian of maximum heat transfer, it is obvious that the instantaneous ablated shape is quite dependent upon model dynamics. Since the dynamic influence is absent from the conventional static test, it follows that the dynamic test offers a meaningful way to evaluate the effects of ablation on the static as well as the dynamic stability of a given configuration.

While physical realism may be enhanced by the testing of unconstrained models, the determination of the aerodynamic loads is no longer a primary measurement as it is in constrained model tests. The primary measurement now is angular displacement from a null or trim condition. In the three-degree-of-freedom gas bearing support, these angles are roll ϕ, pitch (angle of attack) α, and yaw (angle of sideslip) β. The task facing the analyst, then, is to deduce what the loads must have been during the test in order to produce the observed motion. Central to numerically determining aerodynamic loads is a postulating or modeling of the flow-body interaction in the form of ordinary differential equations. The goal of the data reduction process is to determine the numerical values of the coefficients of these differential equations that provide according to some criteria the "best fit" to the observed (measured) angular motion.

In the remainder of this paper we will discuss the mechanical design and construction of the bearing, the data reduction technique, and the wind tunnel testing of ablating and nonablating models.

Bearing Design and Construction

The three-degree-of-freedom gas bearing (TDGB) permits unlimited model freedom in roll and restricted freedom in angles of attack and sideslip. It is certainly possible to provide the same degrees of freedom with a gimbal system using mechanical bearings. However, in the present application where heat loads are modest, a gas bearing is particularly attractive because of its low and consistent friction. The gas bearing does require a continuous supply of gas (air in the present case) and, as it turns out, some control of the tem-

Presented as Paper 82-1367 at the AIAA 9th Atmospheric Flight Mechanics Conference, San Diego, Calif., Aug. 9-11, 1982; submitted Aug. 9, 1982; revision received Jan. 18, 1983.

*Aerospace Engineer, White Oak Laboratory. Associate Fellow AIAA.
†Aerospace Engineer, White Oak Laboratory. Member AIAA.

perature of the gas entering the region of the bearing sphere is necessary to maintain sphere/socket clearances. The bearing air must also exit the model's base; however, the mass flow of the exhaust air is so small that there is no significant effect on model motion.

The sphere/cone is shown attached to the gas bearing and mounted in the NSWC Hypersonic Wind Tunnel in Fig. 1. This model is a 7 deg cone (half angle) with a 22% spherical bluntness (nose radius to base radius).

Figure 2 is an assembly view of the gas bearing housing socket. The front and aft ball housings form the stator of the 6.35 cm (2.5 in.) diam sphere also called the "socket." The inner surface of the housings is molded epoxy (DEVCON). The clearance tolerance between the sphere and the epoxy socket is on the order of 0.0025 cm (0.001 in.). The method of forming this socket and maintaining this tolerance is interesting. When the sphere is fabricated, a second and nearly identical sphere is also fabricated. This second sphere is then nickel-plated. The epoxy socket is then molded to this plated sphere. The unplated sphere then fits the socket with the required clearance. Sphere-socket clearance may vary somewhat so the plating thickness may vary a few thousandths of an inch. However, more important than the clearance itself is consistency in clearance all around the bearing surface. The only difficulty experienced with the bearing clearance was caused by cooled air (due to expansion) which contracted the epoxy after prolonged bearing use. Heating the air prior to entry at the bearing surface totally eliminated this problem.

All components aft of the ball housing are associated with the pitch/yaw/roll fiber optic readout system. This system was not entirely satisfactory, although some angular measurements using the fiber optic system were used for data reduction. Roll or spin rates measured using this system provided a check on the independent measurements which followed from computations of the two oscillatory frequencies.

Bearing air is admitted into the sting at about 2.59 to 2.75×10^6 N/m^2 (375-400 psi). This air should be heated about 20 °C above ambient to prevent significant contraction of the epoxy socket. Setting an exact temperature of the bearing air is not feasible nor is it necessary—the air after expansion in the bearing must be equal to or somewhat greater than the socket temperature. The bearing air supply enters the bearing sphere as indicated and exhausts through eight holes, four forward and four aft. This air is then carried by the bearing exhaust lines in the sphere to the rear of the bearing where it enters the model interior. Bearing exhaust air passes near the fiber optic readout system partially contributing to cooling requirements. It will be noted that there is also water cooling provided to the readout system. The air finally exits the base of the model.

The second air source is the air jet. The air jet is simply a high pressure jet of air [about 5.86×10^6 N/m^2 (850 psi)] which, when applied to one side of the model, impulsively gives the model an initial disturbance in angle and angular rate. Because the model is spinning, a mechanical initiator would be unduly complicated. The air jet has been found to be an entirely reliable and effective means for initiating model motion.

The third and fourth air supplies move the piston and the centering fingers forward and aft. Air at about 3.44×10^5 N/m^2 (50 psi) enters the base through the conduit indicated in Fig. 3. The piston moves forward forcing the centering fingers into the O-ring. The turbine then imparts spin to the model while at the same time holding the model at null in both orthogonal aerodynamic angles. When the desired spin rate is achieved, air is simultaneously bled from the region aft of the piston and applied to the forward piston face by the aft-piston air supply. The model is now available for angle-of-attack initiation by the kicking jet described earlier.

The fiber optic system readout will not be discussed in great detail since it is to be subjected to modification or replacement. The fiber optic light guides are 0.05 cm (0.02 in.) in diameter. These guides are located at discrete angular

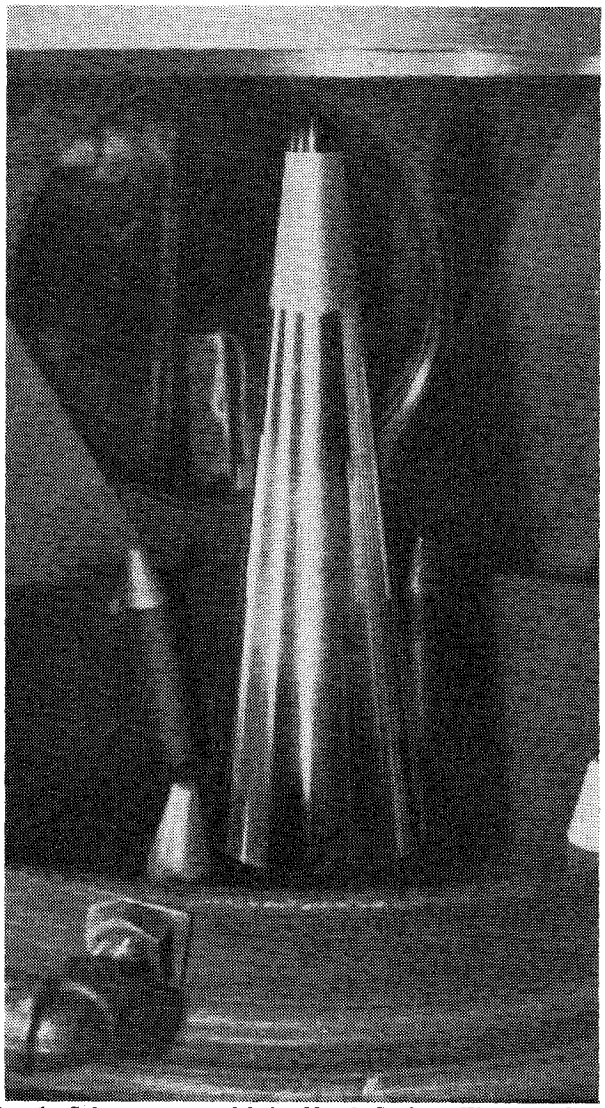

Fig. 1 Sphere-cone model in Naval Surface Weapons Center Hypersonic Wind Tunnel.

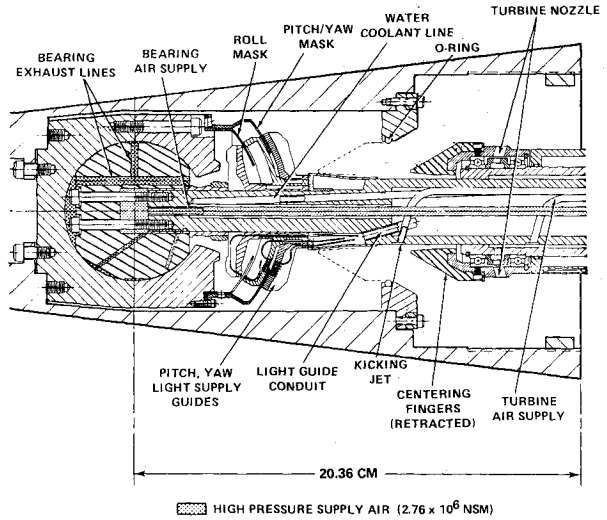

Fig. 2 Air bearing section.

positions. Light from outside the wind tunnel is conducted by the guides through the sting and inside the bearing. The angles of attack (pitch) and sideslip (yaw) are read approximately every half degree; the roll angle is read every 22.5 deg. As the model rotates, a mask covers and uncovers the guides from the external light source. As a guide is uncovered, the light crosses a 0.125 cm (0.050 in.) gap to enter another guide directly opposite the light-carrying guide. The mask sheath (attached to the model and sharing its angular rotation) moves within this gap.

The light from the pickup guide then goes to a photocell where it is converted to an electrical signal. Five channels are required: two for pitch, two for yaw, and one for roll. After these signals have been recorded (analog) on magnetic tape, they are digitized. The digitized signal, together with a "readout algorithm" and calibration, provides the angular record, i.e., degrees (in yaw and pitch) vs time. In the next section, the discussion will cover how this angular record can be used to calculate the characteristic frequencies and damping exponents and ultimately the nondimensional aerodynamic derivatives.

Figure 3 provides a schematic of the more salient features of the various air passages. It may be noted that the sting is not solid but contains various passages for the light guides as well as conduits for bearing and control air. There are five separate air supply passages: bearing, kicking jet, centering fingers-forward, centering fingers-retract, and turbine.

The final air supply drives the turbine. Air is admitted to the turbine at 1.38 to 1.72×10^6 N/m^2 (200-250 psi). The turbine does not contain blades as might be expected, but rather consists of 18 equally spaced holes or nozzles drilled in the piston, forming a ring around the piston. The axes of these nozzles are directed such that the effluent vector has a component tangential to the piston surface. When the piston is pressured in a positive direction, the centering fingers are forced against the O-ring attached to the model. Air imparted to the turbine then spins the model while at the same time holding the model's centerline directly into the wind tunnel flow vector. Once the model has been spun to the desired spin rate, the fingers are retracted, turbine air supply terminated, and the kicking jet initiated. At this point the model is assumed undergoing spin/yaw/pitch motion that is satisfactory for data acquisition.

Since the model must be dynamically balanced for proper angular response, there is provision for insuring that the center of mass is at the point of rotation. Fore and aft movement of the center of mass is controlled by the location of the HEAVIMET (tungsten alloy) balancing slug. Since the model is a body of revolution, most of the components also have an axis of symmetry and are shaped on a lathe. However, internal screw holes and other irregularities can place the center of mass off the configurational axis of symmetry. Consequently, a balancing ring (located at the rear of the model) can be machined in accordance with balancing machine instructions to bring the center of mass laterally to the axis of configurational symmetry.

Because the model is used in a flow environment where the stagnation temperature may be 925°C, prolonged usage might cause the temperature in the vicinity of the fiber optic guides to exceed 85°C. Thus, water cooling is provided by a passage through the center of the sting.

The preceding description covers the essentials of the bearing's mechanical design features. As mentioned earlier, the fiber optic system functioned only intermittently and hence cinematic coverage was used for most of the data acquisition. Tests for maximum sustainable load on the gas bearing have not been made; however, it has shown the capability of sustaining a model weight of 147 Newtons (35 lb) and an axial aerodynamic load of over 440 Newtons (100 lb).

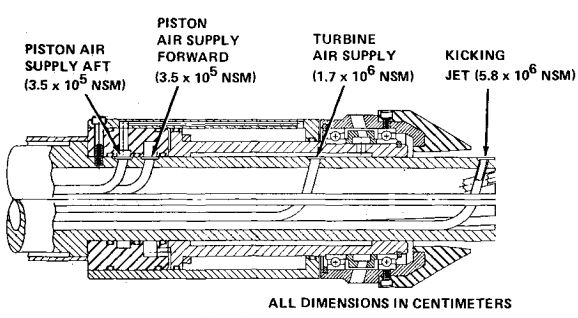

Fig. 3 Air passages.

Data Reduction

Figure 4 depicts the model undergoing angular motion simultaneously about three mutually perpendicular axes while immersed in the hypersonic flow of a continuous medium. It would seem that the physics associated with this angular motion has some similarities with classical aeroballistic motion. However, in the free-flight motion of a projectile there would also be translational motion which would in general have components along the orthogonal axes. Since the wind tunnel model is constrained against linear motion, the three force equations are identically zero, and therefore we need consider only the moment equations.

Relying on the development by Vaughn,[1] it is possible to show that the angular motion of the model about two orthogonal wind tunnel fixed axes is described by the following equations:

$$I\ddot{\alpha}-p\dot{\beta}I_x-M_\alpha\alpha-(M_{\dot\alpha}+M_q)\dot\alpha-M_\delta\delta\cos pt-M_{p\beta}p\beta=0$$

$$I\ddot{\beta}+p\dot\alpha I_x+N_\beta\beta-(N_r-N_{\dot\beta})\dot\beta-M_\delta\delta\sin pt-N_{p\alpha}p\alpha=0 \qquad (1)$$

In the above equations α and β are the angular deviation of the model's axis of symmetry (or principal axis of inertia) from the velocity vector: α is a measure of angular displacement in the vertical plane and β is a measure of angular displacement in the horizontal plane. The dimensional derivatives indicate a proportionality between the pitching and yawing moments, M and N, and angular displacements and rates.

We will now make various assumptions based upon the shape of the model and the magnitude of the angular excursions with an eye to simplifying subsequent analysis. Our

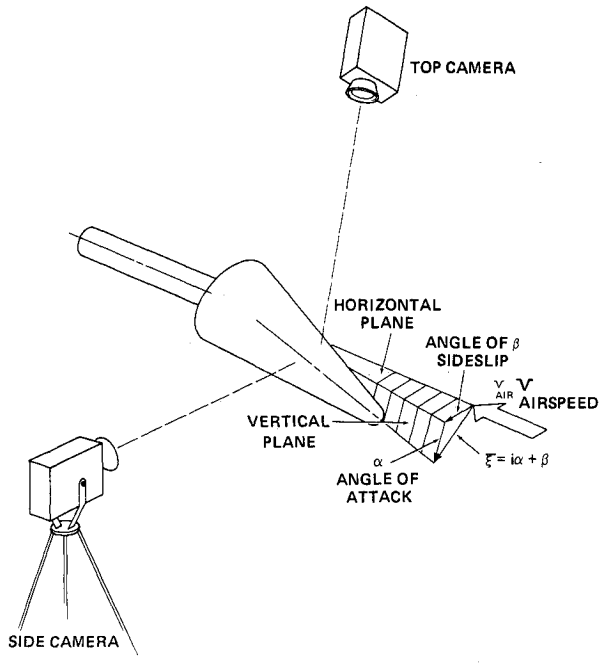

Fig. 4 Orthogonal camera coverage.

main analytic interest at present centers around obtaining a solution of Eqs. (1). First, we will assume that the angular excursions are sufficiently small that there is some merit in describing motion with linear, constant-coefficient equations. Second, we will assume that the roll rate p is constant throughout the test run. Finally, we will make use of the model's rotational symmetry to justify equality between the model's aerodynamic characteristics in yaw and pitch. The consequence of this last assumption is a set of relationships between the yaw and pitch derivatives as,

$$M_\alpha = N_\beta, \qquad M_q = N_r, \qquad M_{\dot\alpha} = -N_{\dot\beta}, \qquad M_{p_\beta} = N_{p_\alpha} \tag{2}$$

Making use of the above three assumptions, Vaughn[1] has shown that the solution to Eqs. (1) may be written as:

$$\alpha = (A_1\cos\omega_1 t + B_1\sin\omega_1 t)e^{\lambda_1 t} + (A_2\cos\omega_2 t + B_2\sin\omega_2 t)e^{\lambda_2 t} + (A_3\cos pt + B_3\sin pt) \tag{3a}$$

$$\beta = (B_1\cos\omega_1 t - A_1\sin\omega_1 t)e^{\lambda_1 t} + (B_2\cos\omega_2 t - A_2\sin\omega_2 t)e^{\lambda_2 t} + (B_3\cos pt - A_3\sin pt) \tag{3b}$$

The constants A_1, B_1, A_2, B_2 are constants of integration and are shown to contain the initial conditions in α, β, $\dot\alpha$, and $\dot\beta$. The constants A_3, B_3 contain the asymmetry moment, $M_\delta\delta$. Although the constants $A_1,\ldots,B_3$ must be numerically evaluated in the data reduction process, such constants have no utility in achieving our goal of assigning numerical values to the stability derivatives of Eqs. (2). For illustrative purposes, the constants A_1 and A_3 are given in Eqs. (4) below, simplified for low damping.

$$A_1 = -\left[\frac{\beta_0 + \omega_2\alpha_0 + (p-\omega_2)A_3}{\omega_1 - \omega_2}\right]$$

$$A_3 = \left[\frac{(M_\delta\delta)/I}{\omega_2(p-\omega_1) + p(\omega_1 - p)}\right]_{p\neq\omega_1} \tag{4}$$

The frequency terms ω_1,ω_2 and the damping exponents λ_1,λ_2 contain the stability derivatives: M_α, the static stability derivative; M_q, the dynamic stability derivative; and M_{p_β}, the Magnus derivative. The derivative $M_{\dot\alpha}$ is assumed negligible in hypersonic flows. The goal, then, of our data reduction efforts will be to obtain numerical values for the following ten constants: A_1, B_1, A_2, B_2, A_3, B_3, ω_1, ω_2, λ_1, λ_2. We note again that only the last four—i.e., ω_1, ω_2, λ_1, λ_2—are of any value in defining the stability derivatives.

Reference 1 contains expressions for ω_1, ω_2, λ_1, λ_2, in terms of the derivatives M_α, M_q, M_{p_β}, roll rate p, and the transverse and axial moments of inertia I and I_x. Since the data reduction process will provide us with numerical values for the frequencies and damping terms, we are more interested at this point in expressing the derivatives in terms of the frequency and damping constants. Such expressions are easily rendered using the development given in Ref. 1:

$$M_\alpha = I\omega_1\omega_2 = C_{m_\alpha}(QSd) \tag{5a}$$

$$M_q = I(\lambda_1 + \lambda_1) = C_{m_q}(QSd^2/2V) \tag{5b}$$

$$p = I/I(\omega_1 + \omega_2) \tag{5c}$$

$$M_{p_\beta} = -\left[\frac{\lambda_1\omega_1 + \lambda_2\omega_2}{\omega_1 + \omega_2}\right]I_x = C_{m_{p_\beta}}(QSd^2/2V) \tag{5d}$$

Equation (5c) contains the interesting assertion that the roll rate need not be measured, but may be deduced from a measurement of the two frequencies, ω_1 and ω_2. Nevertheless, there are at least three advantages in having roll rate available as a measurement. First, the availability of a measured value of roll rate provides a check of sorts on the validity of our data reduction process in that we might expect some agreement between the measured value of roll rate p and that value of p deduced from Eq. (5c). Second, having roll rate available is of some use in setting the initial estimates of the frequencies as required in initiating the iterative data reduction process. Finally, a measured value of roll rate can be used in substantiating the assumption that the roll rate was constant during the test run. The solution of Eqs. (1), given in Eqs. (3), is based upon the assumption of constant roll rate.

The data reduction technique is based upon a variation of the method of least squares called "differential corrections."[2,3] First note that we can obtain analytic values for the angles of attack, α, and sideslip, β, from Eqs. (3). These equations are, in turn, solutions to Eqs. (1), the equations of motion. This analytic value and α and β can be defined at every value of time, $t = t_i$ for which measurements of (α_i, t_i) and (β_i, t_i) are made. In other words, we have a one-to-one correspondence between the analytic values of α and β—i.e., $(\tilde\alpha_i, t_i)$, $(\tilde\beta_i, t_i)$—and the measured values of α and β—i.e., (α_i, t_i), (β_i, t_i). Since our equations will be overspecified, i.e., we have far more data points than the ten constants that we wish to define, we will fit the data with the "best" analytic function having the form given in Eqs. (3). This "best" fit will provide us with numerical values for the ten constants $A_1,\ldots,\lambda_2$. The best fit according to the least-squares criterion is that fit which minimizes the sum of the squares of the difference between the analytic values $(\tilde\alpha_i, t_i)$, $(\tilde\beta_i, t_i)$ and the measured values (α_i, t_i), (β_i, t_i).

It will be noted in Eqs. (3) that the analytic functions $\tilde\alpha$ and $\tilde\beta$ are linear functions of the first six constants $A_1,\ldots,B_3$, but nonlinear functions of the remaining four constants $\omega_1,\omega_2,\lambda_1,\lambda_2$. According to Eqs. (5), it is these last four constants that contain the stability derivatives. Equation (3a) can be expanded in a Taylor series and truncated after the first two terms. [All of the following remarks apply equally to Eq. (3b).] Thus,

$$\tilde\alpha_i = \tilde\alpha_{0i}(t_i, \bar A_1,\ldots,\bar\lambda_2) + \frac{\partial\tilde\alpha}{\partial A_1}A_1 + \ldots + \frac{\partial\tilde\alpha}{\partial\lambda_2}\lambda_2 \tag{6}$$

where $\bar A_1,\ldots,\bar\lambda_2$ are estimated values of the ten constants and $A_1,\ldots,\lambda_2$ are now defined as corrective values used to improve the estimates. Thus, we will first assume values for $A_1,\ldots,\lambda_2$ and then carry out the differential corrections procedure to obtain the correxive values. We will then use these corrective values to update our estimates by algebraically adding corrective values to the previous estimates as,

$$\bar A_1 + A_1 \rightarrow \bar A_1 \tag{7}$$

We may now write Eq. (6) as

$$\tilde\alpha_i = \tilde\alpha_{0i} + H_i\bar u \tag{8}$$

where

$$H_i = \left[\frac{\partial\tilde\alpha_i}{\partial A_1},\ldots,\frac{\partial\tilde\alpha_i}{\partial\lambda_2}\right], \qquad \bar u = [A_1,\ldots,\lambda_2]^T \tag{9}$$

The residual r_i is defined as the difference between the analytic estimate $\tilde\alpha_i$ of Eq. (6) and the data point α_i as

$$r_i = \alpha_i - \tilde\alpha_i = \tilde\alpha_i - \alpha_{0_i} - H_i\bar u = R_i - H_i\bar u \tag{10}$$

Note that R_i is the difference between the estimate $\tilde\alpha_{0i}$ and the data point α_i. Now r_i and R_i are single numbers so they may be regarded as elements in a $(n,1)$ vector, where n is the number of data points: H_i is a (1,10) matrix and $\bar u$ is a (10,1) matrix. If we regard H_i as the row of $(n,10)$ matrix, we may

rewrite Eq. (10) as,

$$\bar{r} = \bar{R} - H\bar{u} \tag{11}$$

The sum of the squares of the residuals is obviously

$$\bar{r}^T\bar{r} = (R - H\bar{u})^T(\bar{R} - H\bar{u}) \tag{12}$$

The goal of our data reduction process is to find the values of $\bar{u}$, say $\hat{u}$, which minimizes the sum of the squares of the residuals, as

$$\frac{\partial}{\partial \bar{u}}(\bar{r}^T\bar{r}) = \frac{\partial}{\partial \bar{u}}[(\bar{R} - H\bar{u})^T(\bar{R} - H\bar{u})] = 0 \tag{13}$$

Assuming that the Hessian of $(\bar{r}^T\bar{r})$ is positive semidefinite, the differentiation indicated in Eq. (13) will provide us with an equation for the vector $\hat{u}$ which minimizes $(\bar{r}^T\bar{r})$. This equation may be shown to be,

$$\hat{u} = (H^TH)^{-1}H^T\bar{R} \tag{14}$$

The above equation is suitable for planar motion only, e.g., motion in the vertical or angle-of-attack plane. If we have biplanar motion, then we must include a development similar to that given previously for Eq. (3b). If q_i is the residual for the side-slip equation, L is the derivative matrix corresponding to matrix H, and $\bar{Q}$ is the residual matrix corresponding to $\bar{R}$, we must minimize the sum of the squares of the angle of attack and the sum of the squares of the angle of side-slip residuals. Thus, we would require the following derivative to be set to zero:

$$\frac{\partial}{\partial \bar{u}}[\bar{r}^T\bar{r} + \bar{q}^T\bar{q}] = 0 \quad \text{or} \quad \frac{\partial}{\partial \bar{u}}[(\bar{R} - H\hat{u})^T(\bar{R} - H\hat{u}) + (\bar{Q} - L\hat{u})^T(\bar{Q} - L\hat{u})] = 0 \tag{15}$$

The result is the following equation for the improvement in the estimates of the ten parameters $\bar{u} = (A_1, \ldots, \lambda_2)^T$:

$$\hat{u} = (H^TH)^{-1}H^T\bar{R} + (L^TL)^{-1}L^T\bar{Q} \tag{16}$$

The procedure then is to estimate the ten parameters, $\bar{u} = (A_1, \ldots, \lambda_2)^T$, solve Eq. (15) for $\hat{u}$, and then improve the estimates by replacing $(\bar{A}_1, \ldots, \bar{\lambda}_2)^T$ by $(\bar{A}_1 + A_1, \ldots, \bar{\lambda}_2 + \lambda_2)$ according to Eq. (7). Once the iterative procedure has converged sufficiently (according to some criterion), the estimates in the final iteration become the best estimates for $\bar{u}$. Now the constants $\omega_1, \omega_2, \lambda_1, \lambda_2$ are available for computing the stability derivatives according to Eqs. (5).

Wind Tunnel Tests

A series of wind tunnel tests were carried out using both ablating and nonablating models. Prior to ablation, the models had an identical configuration: a 7 deg half-angle cone with a bluntness ratio of 0.223 and an axis of rotation (moment reference center) of 0.595 body lengths aft of the unablated nose (see Fig. 5).

The testing procedure was fairly straightforward. With the model mounted in the wind tunnel, the spin turbine was activated with 3.45×10^5 N/m^2 (50 psi) applied to the piston-forward conduit. The tachometer reading was used to monitor the roll rate. When the desired roll rate was reached and maintained, the orthogonal cameras were put into operation, the clutch disengaged, and the kicking-jet activated. Because it is not possible to visually examine the model during the test, the outputs from both angular transducers were entered in the XY jacks of an oscilloscope. The display is a rough portrait of the $\alpha\beta$ motion of the model.

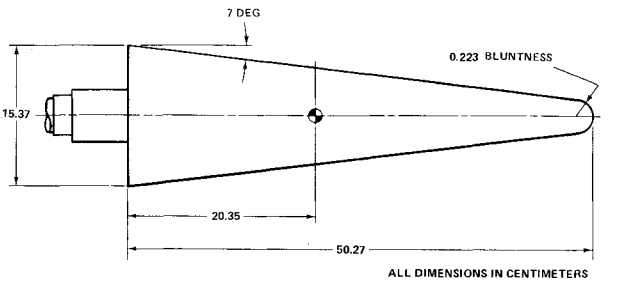

Fig. 5 Model dimensions.

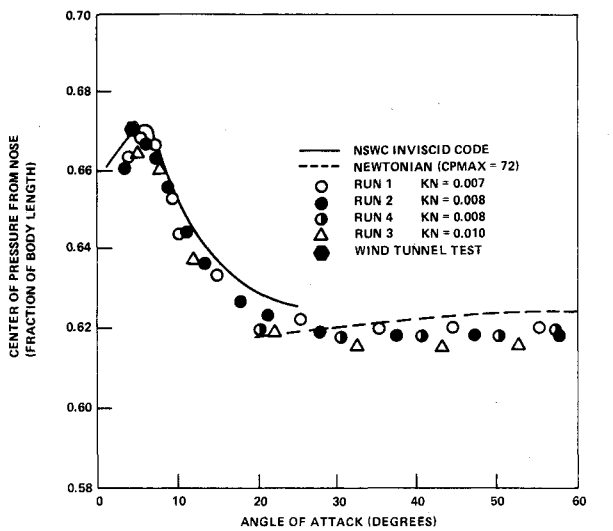

Fig. 6 Comparison of dynamic wind tunnel test with static wind tunnel tests (1, 2, 3, 4).

In the nonablating tests, the 7 deg conical model was tested with a steel hemispherical nose in place. The data reduction program provided a static pitching moment derivative C_{m_α} of -0.328. The static center of pressure aft of the nose in fractions of body length L is given by the following relationship:

$$\bar{x} = \frac{x}{L} = \left(\frac{C_{m_\alpha}}{C_{N_\alpha}}\right)\left(\frac{D}{L}\right) + 0.595 \tag{17}$$

With a body length of 50.165 cm (19.75 in.), a maximum body diameter of 15.378 cm (6.054 in.), and a normal force derivative C_{N_α} of 1.35, the center of pressure is 0.669 body lengths aft of the "body vertex." There are no published data applicable to this configuration at a Mach number of 7.95. However, Fig. 6, taken from Ref. 4, is a reproduction of some static center of pressure data measured at Mach 10.

It will be noted that the furthest aft that the center of pressure reaches is about 0.67 body lengths. As just noted, the center of pressure measured in these dynamic tests is at 0.669 body lengths. It is not possible to compare the static (constrained) test results with dynamic tests since the angle of attack changes continuously during the dynamic test: the dynamic testing took place over an angle-of-attack range of about 3 deg. Taking an rms value of something like 2 deg, it may be seen that correlation of the center of pressure between the two techniques is quite satisfactory. The results of these nonablating tests may be concluded with a listing of the stability derivatives and roll rate reduced from the angular history as follows: $C_{m_\alpha} = -0.328$; $C_{m_q} = -1.6$; $C_{m_{p\beta}} = +0.16$, and $p = 29.9$ rad/s.

For the ablating model test the hemispherical nose was removed and replaced by a camphor nose, also hemispherical, but molded over a steel biconic substructure. The shape of this

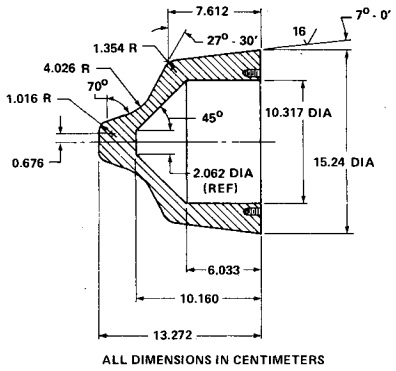

Fig. 7 Ablating nose substructure.

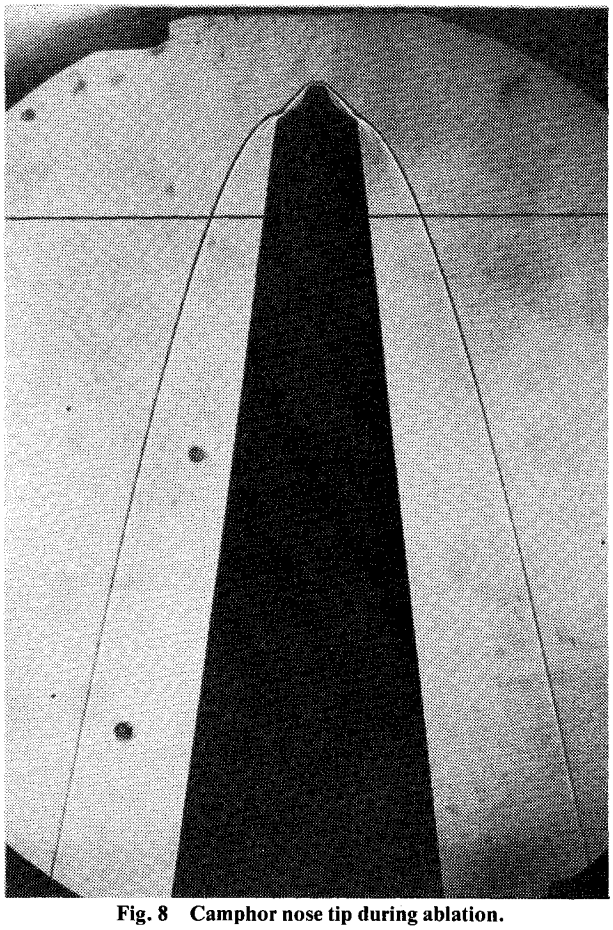

Fig. 8 Camphor nose tip during ablation.

substructure, shown in Fig. 7, was derived from an experimental program discussed in Ref. 5.

The camphor nose ablates to this biconic substructure in about 30-40 s. Figure 8 is a photograph of the partially ablated camphor nose. It will be noted that while the steel substructure is not yet exposed, the originally hemispherical shape is giving evidence of the biconic shape seen in Fig. 7.

Because the ablating model's shape is not constant, we might expect that the stability derivatives will change throughout the test. In anticipation of changing aerodynamic characteristics, the 750 or so data points of the entire ablation run were separated into overlapping subintervals of 50 data points.

The first 50 data points of the ablation test are shown as an (α-β) plot in Fig. 9. It will be noted that during the approximately 2-s duration of this 50-point record, the model went through about four oscillations. We also note the coupling of the roll rate with the angular oscillations by the rotation of the plane of oscillation.

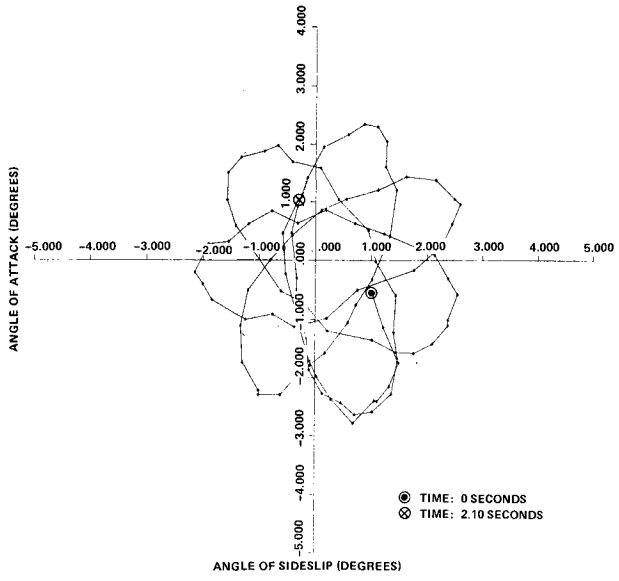

Fig. 9 Angle of attack vs angle of sideslip (ablating nose).

The measurements indicated that the pitching moment derivative C_{m_α} experienced a monotonic reduction (in magnitude) with time as ablation proceeded. If a constant value for the normal force derivative C_{N_α} is assumed, then the preceding observation is equivalent to recognizing that the center of pressure moved steadily forward toward the nose as ablation continued. Initially, the center of pressure was measured at 0.073 body lengths aft of the rotation point. At the completion of ablation, the center of pressure was at 0.054 body lengths. The center of pressure measured earlier on a static (constrained) model was close to the theoretical value of 0.053. It should be remembered that the model in the dynamic test was undergoing motion in three degrees of freedom and that the windward meridian was constantly changing in body coordinates.

A description of the dynamic characteristics is much more complicated. At the beginning of ablation the angular record indicated dynamic stability. About 1 s after the start of the record, the motion became dynamically unstable until about 2 s elapsed. After 2 s the motion became stable again. This alternate dynamic stability/instability continued throughout the record. Further discussion of the model's dynamic behavior is contained in Ref. 3. A postablation test was also conducted during which the biconic shape of Fig. 7 was in place. Measurements during these tests located the center of pressure at 0.0544 body lengths. It was also noted that in spite of the absence of ablation, there was again evidence of periods of dynamic stability alternating with dynamic instability.

Another series of ablation/postablation testing was carried out with a tilted nose replacing the symmetrical biconic nose of Fig. 7. The tilted nose was formed by setting the centerline of the biconic nose 3 deg to the centerline of the conical afterbody. These tests produced results similar to those just described for the symmetrical nose: a forward moving center of pressure and periods of dynamic instability. Further details are contained in Ref. 3.

The interesting question raised by these tests is the effect of nosetip ablation in causing dynamic instabilities. The tests reported in this paper have indicated that nosetip ablation does cause dynamic instabilities, in concurrence with the conclusions of Ericsson and Reding.[6] "A slender conical reentry body may experience increased static stability but severely decreased dynamic stability at low angles of attack and low oscillation amplitudes when ablation is concentrated to the blunted nose and cone trailing edge."

Ericsson and Reding's paper is an analytic exercise and is not substantiated by any experimental results. The authors

admit in the conclusion to their paper: "...the analysis presented herein is highly speculative...."

Nevertheless, to some extent the conclusions of Ref. 6, as indicated by the above quotation seem to be substantiated by the results of the ablating nose test reported herein.

In 1965 a series of experiments were carried out to examine the dynamic behavior of an ablating model undergoing single-degree-of-freedom angular (pitch) motion. These experimental results were reported in what may be regarded as the seminal paper in the experimental investigations of the effects of surface ablation on the dynamics of a re-entry body.[7] While this paper by Grimes is based upon wind tunnel dynamic tests, it should be appreciated that there are considerable differences between the model support system used in Grimes' experiments and the three-degree-of-freedom gas bearing. The model in Grimes' experiments of Ref. 7 does not roll and its angular motion is restricted entirely to a plane. By way of contrast the model in the three-degree-of-freedom gas bearing tests as reported herein is free, within an upper bound restriction on the total angle of attack, to undergo simultaneous and mechanically uncoupled yaw, pitch, and roll motion. In other words, a comparison is being made between experimental results from single-degree-of-freedom and three-degree-of-freedom supports. Clearly there must be a considerable difference between the ablation physics in both cases. In the three-degree-of-freedom support the presence of roll rate allows the region of ablation to alter its orientation with respect to the velocity vector independent of the angle of attack. Consequently, neither Grimes' nor Ericsson's paper for that matter can be entirely supportive of the gas bearing tests presented in this paper. Indeed there seems to be some conflict between Ericsson and Grimes as to the effect of ablation on dynamic stability. The following quotation is taken from Grimes' paper which conflicts with the experimental results reported herein and with the analytic results of Ericsson as indicated by the previously given quotation. From Ref. 7 we have: "Coating the entire model...forward of the center of gravity, produced a dynamically stable configuration with C_{m_q} values approaching those for flight test. Coating the rearward sections of a conic or cone-cylinder flair produces a dynamically unstable model." In this quotation the word "coating" refers to the application to the model of a low-temperature ablator such as paradichlorobenzine $C_6H_4C_2$.

Conclusions

The following is a partial listing of the conclusions that might be drawn from these ablation tests:

1) The static center of pressure is at about 0.073 body lengths aft of the center of gravity (0.595 body lengths aft of the nose) at the beginning of ablation. This value is essentially the same as that measured for the steel nose (nonablating) sphere cone model.

2) The static center of pressure moved forward during ablation to a value of about 0.054 body lengths.

3) Agreement seems to be acceptable with results from supported testing where the center of pressure is about 0.053 body lengths. It must be remembered that dynamic testing about a single axis cannot provide the normal force derivative, C_{N_α}; hence, a final evaluation of the center of pressure must rely on an external source of C_{N_α}.

4) Dynamic measurements indicated regions of dynamic stability and instability. No convincing argument is available at this time to entirely explain this observation.

References

[1] Vaughn, H.R., "A Detailed Development of Tricyclic Theory," Rept. SC-M-67-2933, Sandia Laboratories, Albuquerque, N. Mex., Feb. 1968.

[2] Nielsen, K. L., *Methods in Numerical Analysis,* 2nd ed., The Macmillan Company, New York, N.Y., 1964, pp. 309-313.

[3] Regan, F.J., "Dynamic Testing with the NSWC Three-Degree-of-Freedom Gas Bearing" NSWC TR 81-491, March 1982.

[4] Ragsdale, W.C., et al., "Mach 10 IAP Static Force Test Program in the NSWC/WOL Hypersonic Tunnel (WTR 1296)," NSWC/WOL MP-77-33, Sept. 1977.

[5] Jobe, M.D. et al., "Bi-Modal Flow Field Feasibility Demonstration in the NSWC/WOL Hypersonic Tunnel (WTR 1319)," NSWC MP-79-217, May 1979.

[6] Ericsson, J.E., and Reding, J.P., "Ablation Effects on Vehicle Dynamics," *Journal of Spacecraft and Rockets,* Vol. 3, Oct. 1966, pps. 1476-1483.

[7] Grimes, J.H.Jr. and Casey, J.J., "Influence of Ablation on the Dynamics of Slender Re-entry Configurations," *Journal of Spacecraft and Rockets,* Vol. 2, No. 1, Jan./Feb. 1965, pp. 106-107.